

Recurrent convolutional neural networks for non-adiabatic dynamics of quantum-classical systems

Alex P. Ning,^{1,2} Lingyu Yang,³ and Gia-Wei Chern³

¹*Department of Computer Science, University of Virginia, Charlottesville, Virginia, 22904, USA*

²*Department of Mathematics, University of Virginia, Charlottesville, Virginia, 22904, USA*

³*Department of Physics, University of Virginia, Charlottesville, Virginia, 22904, USA*

(Dated: December 10, 2024)

Recurrent neural networks (RNNs) have recently been extensively applied to model the time-evolution in fluid dynamics, weather predictions, and even chaotic systems thanks to their ability to capture temporal dependencies and sequential patterns in data. Here we present a RNN model based on convolutional neural networks for modeling the nonlinear non-adiabatic dynamics of hybrid quantum-classical systems. The dynamical evolution of the hybrid systems is governed by equations of motion for classical degrees of freedom and von Neumann equation for electrons. The physics-aware recurrent convolutional (PARC) neural network structure incorporates a differentiator-integrator architecture that inductively models the spatiotemporal dynamics of generic physical systems. Validation studies show that the trained PARC model could reproduce the space-time evolution of a one-dimensional semi-classical Holstein model with comparable accuracy to direct numerical simulations. We also investigate the scaling of prediction errors with size of training dataset, prediction window, step-size, and model size.

I. INTRODUCTION

Recurrent Neural Networks (RNNs) are an established framework for analyzing sequential or dynamic data with applications across physics [1–4]. Unlike feed-forward networks, which assume independence between inputs, RNNs incorporate internal feedback loops which can capture dependencies between sequential data. This is a crucial behavior when modeling the evolution of time-dependent physical systems and trajectories with strong temporal correlations between data points. RNNs can learn the underlying dynamics from time-series data without requiring explicit knowledge of governing equations. They can predict future states of a system based on its past behavior. Indeed, RNN is among one of the prominent deep-learning approaches often employed to solve partial differential equations (PDEs) [5–18], which are the ubiquitous tools for modeling the spatiotemporal evolution of most physical systems.

The essential idea behind the RNN approach to PDE, namely using current and previous step states to calculate the state at the next time step, is actually similar to most time-stepping numerical methods for solving time-dependent PDEs, such as Euler’s, Crank-Nicolson, and higher-order Runge-Kutta schemes [19–21]. The RNN serves as a surrogate time-stepping method replacing the numerical finite-difference or finite-element schemes. The numerical solution on each of the grid point (for finite difference) or grid cell (for finite element) computed at a set of contiguous time points can be treated as a time sequence data for training a multi-input RNN. Standard supervised learning methods are used to optimize the parameters of neural network layers through learning the numerical solutions on the grids.

The dynamics of physical systems is also characterized by the emergence of complex spatial patterns, such as

stripes and vortices. This indicates the importance of spatiotemporal correlations in the dynamical modeling of such physical systems. Yet, traditional neural networks often perform poorly at capturing local relationships due to their fully-connected nature, Convolutional Neural Networks (CNNs) [22], on the other hand, excel at such tasks. CNNs are a variety of neural network which utilize *convolution* layers to process a grid or array of values using a “sliding” *kernel* to extract learned features with geometric structure. Convolution layers strongly exploit patterns with geometric locality in inputs, and within a CNN many convolution layers are often composed to extract a hierarchy of features starting from low-level patterns to high-level and complex relationships. Because of these unique capabilities, CNNs have become a crucial component in deep-learning approach to solving PDEs [15–18].

The recently proposed RNN, dubbed physics-aware recurrent convolution (PARC) [17, 18], further incorporates physics information into its architecture, thus offering improved accuracy and representation capability. Indeed, machine learning (ML) models with physical constraints explicitly incorporated have attracted great interest among researchers. For example, the ML force-field framework for *ab initio* molecular dynamics utilizes the locality principle to implement local energy or force models, enabling linear scaling computation [23–29]. Another example is the equivariant neural networks which allows physical symmetries to be explicitly included on a supervised learning model. Their architecture is designed in such a way that the neurons of each layer exhibit well-defined transformation properties under operation of a given symmetry group [30–33].

Compared with other RNNs, PARC is structured as two separate but directly connected CNN-based differentiator and integrator components. The two-stage architecture is motivated by algorithms of most numeri-

cal methods for PDEs: the derivatives of the field $d\mathbf{u}/dt$ are first computed from the current configuration, which is then integrated to produce the future states of the evolving field. The stand-alone integral solver also offers the capability for stable, longer time predictions. This differentiator-integrator structure of PARC thus provides a prior on integration tasks, resulting in its “physics-aware” nature and enabling improved data efficiency and performance.

In this work we propose a deep-learning approach based on the PARC architecture for modeling the non-adiabatic dynamics of lattice models with coexisting classical and quantum electron degrees of freedom. Such hybrid quantum-classical models are an important simplification for modeling realistic physical systems with, e.g. multiple length and time scales. One of the most prominent examples is the *ab initio* molecular dynamics methods widely used in quantum chemistry and materials science [34]. Yet, direct dynamical simulation of such hybrid systems is still a challenging computational task because of the exponentially large dimension of the Hilbert space associated with the quantum subsystem.

Even in the absence of direct electron-electron interactions, a many-body description of electrons is still required in order to accommodate the Fermi-Dirac quantum statistics. In the non-interacting case, the complexity of simulating a many-electron wave function can be reduced to the dynamics of single-electron density matrix or correlation functions $\rho(\mathbf{r}, \mathbf{r}', t)$ where \mathbf{r}, \mathbf{r}' are coordinates of lattice sites. As a result, for a D -dimensional system $\mathbf{r} \in \mathbb{Z}^D$, the minimum description in terms of density matrix requires a $2D$ -dimensional time-dependent differential equations. As a proof-of-principle, here we consider the 1-dimensional (1D) semiclassical Holstein model and build a PARC framework to model its non-adiabatic dynamics under a quantum quench. By employing a recurrent next-step prediction approach, we show that the PARC model can accurately perform multi-step integration from any given starting point. Furthermore, we examine error accumulation during successive recurrent predictions, as well as the scaling effects of data step size, training set size, and model size on prediction accuracy.

Although the dynamics of discrete lattice systems is formally described by coupled ordinary differential equations (ODEs), spatial couplings between dynamical variables nonetheless resemble those of discretized PDEs using either finite-difference or finite-element schemes. The spatial correlations and potential emergent spatial patterns can be efficiently captured by the CNN built in PARC, as discussed above. Indeed, similar CNN-based force-field models have been developed for spin dynamics of the so-called s-d system, a lattice model of metallic magnets [35]. Importantly, the convolution operation with a finite-sized kernel naturally incorporates the locality principle into the PARC model, which can be straightforwardly scaled to larger systems.

Before closing the Introduction section, we note that PARC relies on the inductive bias method [36] to embed

prior physics knowledge within the neural network structures. This is in contrast to the Physics-Informed Neural Networks (PINNs) [37], a popular deep-learning architecture for solving PDEs, which are based on learning-biased approach where physical constraints are directly enforced by minimizing the PDE residues and boundary/initial conditions through a loss function. Although PINNs can achieve high performance with no training data besides the initial condition, a single PINN is in general only capable of approximating the solution to a single initial condition, making it unfit for the generalized task of integration on a family of solutions.

The rest of the paper is organized as follows. In Sec. II, we discuss the non-adiabatic dynamics of the semiclassical Holstein model, within the Ehrenfest dynamics framework. After a brief review on the PARC formulation, the modified recurrent architecture for modeling the dynamics of Holstein model is presented in Sec. III. The results and several benchmark analyses are discussed in Sec. IV. Finally we present a summary and outlook in Sec. V.

II. NON-ADIABATIC DYNAMICS OF HOLSTEIN MODEL

We consider a 1D Holstein model [38] with spinless fermions, described by the following Hamiltonian with three parts

$$\begin{aligned} \hat{\mathcal{H}} = & -t_{\text{nn}} \sum_i \left(\hat{c}_i^\dagger \hat{c}_{i+1} + \hat{c}_{i+1}^\dagger \hat{c}_i \right) - g \sum_i \left(\hat{n}_i - \frac{1}{2} \right) \hat{Q}_i \\ & + \sum_i \left(\frac{1}{2m} \hat{P}_i^2 + \frac{1}{2} m \Omega^2 \hat{Q}_i^2 \right). \end{aligned} \quad (1)$$

Here \hat{c}_i^\dagger (\hat{c}_i) denotes the creation (annihilation) operator of an electron at lattice site- i , Q_i represents a local phonon degree of freedom, P_i is the associated conjugate momentum, m is an effective mass, Ω is the intrinsic oscillation frequency, and $K \equiv m\Omega^2$ is the force constant, finally g denotes the electron-phonon coupling coefficient. The first term $\hat{\mathcal{H}}_e$ describes the hopping of electrons between nearest neighboring sites. The second part essentially describes the Einstein phonon model, which corresponds to a set of simple harmonic oscillators each associated with a lattice site. The third term describes a local coupling between the electron density $\hat{n}_i = \hat{c}_i^\dagger \hat{c}_i$ and the displacement of the oscillator.

The Holstein model at half-filling on various bipartite lattices exhibits a robust commensurate CDW order that breaks the sublattice symmetry [39–42]. In one dimension, this commensurate CDW order is characterized by an ultra-short period modulation of electron density,

$$\langle n_i \rangle = \bar{n} + \delta n \cos\left(\frac{\pi}{a} x_i\right), \quad (2)$$

where $\langle \dots \rangle$ denotes ground-state expectation value, $\bar{n} = 1/2$ is the average density, δn is the modulation amplitude, a is the lattice constant, and $x_i = x_0 + i a$ is the

physical coordinate of site- i . It is worth noting that the CDW order remains robust even in the semiclassical approximation. Indeed, the semiclassical phase diagram of the CDW order obtained by a hybrid Monte Carlo method agrees very well with that obtained from determinant quantum Monte Carlo simulations [42]. Within the semiclassical approximation for the CDW dynamics, the Holstein is an example of the hybrid quantum-classical systems discussed above.

Here we employ the Ehrenfest dynamics framework [34, 43] to describe the semiclassical dynamics of the Holstein model. A similar semiclassical dynamics method was recently employed to study the photo-emission and long-time behaviors of CDW states in the 1D Holstein model [44]. To this end, we assume a product form for the quantum state of the system: $|\Gamma(t)\rangle = |\Phi(t)\rangle \otimes |\Psi(t)\rangle$, where $|\Phi(t)\rangle$ and $|\Psi(t)\rangle$ denote the phonon and electron wave-functions, respectively. The semi-classical approximation for the lattice subsystem amounts to a direct product wave function $|\Phi(t)\rangle = \prod_i |\phi_i(t)\rangle$ for the phonons. As a result, the expectation value of phonon operators, e.g. $\langle \Gamma(t) | \hat{Q}_i | \Gamma(t) \rangle$ reduces to $Q_i(t) \equiv \langle \phi_i(t) | \hat{Q}_i | \phi_i(t) \rangle$, and similarly for the momentum operators, $P_i(t) \equiv \langle \Gamma(t) | \hat{P}_i | \Gamma(t) \rangle = \langle \phi_i(t) | \hat{P}_i | \phi_i(t) \rangle$.

The dynamics of these ‘classical’ variables is given by the expectation of Heisenberg equation, e.g. $d\langle P_i \rangle / dt = -i\langle [\hat{P}_i, \hat{\mathcal{H}}] \rangle / \hbar$, where $\langle \dots \rangle$ is the expectation value computed using the full wave-function $|\Gamma(t)\rangle$. Direct calculation of the commutators yields the coupled Hamiltonian dynamics

$$\frac{dQ_i}{dt} = \frac{P_i}{m}, \quad \frac{dP_i}{dt} = gn_i - KQ_i. \quad (3)$$

Here the time-dependent electron density is given by $n_i(t) = \langle \Gamma(t) | \hat{n}_i | \Gamma(t) \rangle$, which can be simplified to $n_i(t) = \langle \Psi(t) | \hat{n}_i | \Psi(t) \rangle$ thanks to the product form of the system quantum state.

Since the Holstein Hamiltonian is quadratic in electron operators, the time evolution of the many-electron Slater-determinant wave function can be exactly solved numerically. A more efficient approach is based on the dynamical equation for the single-particle density matrix,

$$\rho_{ij}(t) = \langle \Psi(t) | \hat{c}_j^\dagger \hat{c}_i | \Psi(t) \rangle. \quad (4)$$

The on-site electron number, which is a driving force of the lattice dynamics in Eq. (3), is readily given by the diagonal elements: $n_i(t) = \rho_{ii}(t)$. The dynamical evolution of the density matrix is governed by the von Neumann equation

$$\frac{d\rho}{dt} = -i[H(\{Q_i\}), \rho], \quad (5)$$

where H is a matrix which can be viewed as the first-quantized Hamiltonian on a lattice. Explicitly, $H_{ij} = -t_{nn}(\delta_{j,i+1} + \delta_{j,i-1}) - g\delta_{ij}Q_i(t)$. Direct calculation gives

$$i\hbar \frac{d\rho_{ij}}{dt} = \sum_k (\rho_{ik}t_{kj} - t_{ik}\rho_{kj}) + g(Q_j - Q_i)\rho_{ij}. \quad (6)$$

There are two characteristic time scales for the dynamics of the Holstein model. First, from the bandwidth of the electron tight-binding model $W = 4t_{nn}$, one can define a time scale $\tau_e = \hbar/t_{nn}$ for the electron dynamics. Another time scale is given by the natural frequency Ω of the local simple harmonic oscillator: $\tau_L = 1/\Omega$. The dimensionless adiabatic parameter is defined as the ratio $r = \tau_e/\tau_L = \hbar\Omega/t_{nn}$. The electron-phonon coupling can also be characterized by a dimensionless parameter λ as follows. First, let Q^* be lattice distortions estimated from the balance of elastic energy and electron-phonon coupling: $KQ^{*2} \sim g\langle n \rangle Q^*$. Assuming electron number $\langle n \rangle \sim 1$, we obtain $Q^* \sim g/K$. The dimensionless parameter $\lambda = gQ^*/W = g^2/WK$ corresponds to the ratio of electron-phonon coupling to the bandwidth. For all simulations discussed below, the adiabatic parameter is set to $r = 0.4$. The simulation time is measured in unit of τ_e , energies are measured in units of t_{nn} , and the lattice distortion is expressed in terms of Q^* .

III. PARC NEURAL NETWORK FOR HOLSTEIN MODEL

In this section we present a PARC neural network for modeling the non-adiabatic dynamics of the 1D semiclassical Holstein model. While the state of the simple harmonic oscillators on a chain is described by two 1D arrays $\{Q_i\}$ and $\{P_i\}$, the minimum dynamical variables for the many-electron system are given by a density matrix ρ_{ij} , due to the quantum Fermi-Dirac statistics. This means that, for the simpler case of non-interacting electrons, the 1D quantum dynamics can be effectively modeled by an effective 2D classical dynamics.

A. PARC: a brief review

We first briefly review the basic principles of PARC, our presentation closely follows that in Ref. [17]. By introducing a state vector $\mathbf{u} = [Q_i, P_i, \rho_{ij}]$, the semiclassical dynamics of the Holstein model can be cast into a form of the standard ordinary differential equation:

$$\frac{d\mathbf{u}}{dt} = \mathcal{F}(\mathbf{u}), \quad (7)$$

with proper initial conditions for each components of \mathbf{u} . Here we consider only time-invariant differential systems, which applies to our case of Holstein model. By introducing a discrete time interval Δt , an RNN model can be trained to predict the state vector $\mathbf{u}(t + \Delta t)$ at the next time step with the current state $\mathbf{u}(t)$ as the input. Instead of building a single neural network to provide this mapping, PARC introduces two CNNs, corresponding the differentiator and integrator steps of a finite-difference method for solving differential equation. This is motivated from the integration of the differential

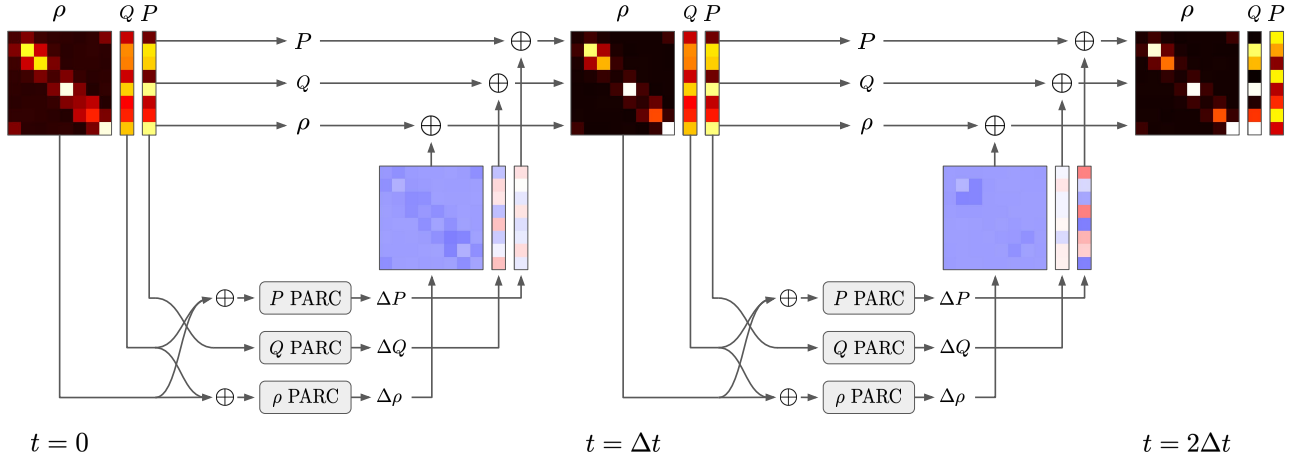


FIG. 1. Schematic diagram of the recurrent structure for non-adiabatic dynamics of the semiclassical Holstein model. The framework is based on three PARC neural networks, one for each of the three dynamical degrees of freedom: Q , P , and ρ . Each of the three PARC neural nets is composed of a differentiator CNN and an integrator CNN.

equation over a finite time interval Δt

$$\mathbf{u}(t + \Delta t) = \mathbf{u}(t) + \int_t^{t+\Delta t} \mathcal{F}(\mathbf{u}) dt, \quad (8)$$

By introducing an integrator operator as a functional:

$$\mathcal{S}(f) = \int_t^{t+\Delta t} f(\mathbf{u}) dt, \quad (9)$$

The increment of the state vector over Δt can then be expressed as to composition of differential operator $\mathcal{F}(\mathbf{u})$ and the implicit integral operator. As both are mathematical operators, they can be accurately modeled by CNN as suggested by the universal approximation theorem [45]. The mapping over one time-step is then approximated by

$$\mathbf{u}(t + \Delta t) = \mathbf{u}(t) + \mathcal{S}[\mathcal{F}[\mathbf{u}(t) | \phi] | \theta]. \quad (10)$$

where $\mathcal{F}[\cdot | \phi]$ and $\mathcal{S}[\cdot | \theta]$ are the CNN approximation to the differentiator and integrator operators, respectively, with ϕ and θ being their respective trainable parameters.

Based on this physics motivated architecture, there are two contributions to the loss function for training the neural networks

$$L(\phi, \theta | \hat{\mathbf{u}}) = \sum_t \|d\hat{\mathbf{u}}/dt - \mathcal{F}[\mathbf{u} | \phi]\|_2 + \sum_t \|\hat{\mathbf{u}}(t + \Delta t) - \mathbf{u}(t) - \mathcal{S}[\mathcal{F}[\mathbf{u} | \phi] | \theta]\|_2, \quad (11)$$

where $\hat{\mathbf{u}}(t)$ denotes the ground-truth trajectory of the state vector obtained from direct numerical simulations.

B. Implementation and training details

Next we discuss details of the implementation. A schematic diagram of the recurrent structure of our

PARC-based model is shown in FIG. 1. A PARC neural network is constructed for each of the three dynamical variables Q , P , and ρ . For the electron density matrix ρ , we utilize a complex-valued 2-dimensional PARC CNN, denoted as \mathcal{N}_ρ . For both Q and P , we use (separate) real-valued 1-dimensional PARC CNNs, denoted as \mathcal{N}_Q and \mathcal{N}_P respectively. Note that each of these neural networks is a composite of the differentiator and integrator: $\mathcal{N} = \mathcal{S} \circ \mathcal{F}$. The input/output structure of the three PARC networks is determined by the governing dynamical equations. For example, since the derivative dQ/dt only depends on the conjugate momentum, as shown in the equation of motion Eq. (3), the input to \mathcal{N}_Q is the momentum array P . The mapping of the three PARC neural nets is summarized here

$$\begin{aligned} Q_{\text{pred}}(t + \Delta t) &= \mathcal{N}_Q [P(t) | \phi_Q, \theta_Q], \\ P_{\text{pred}}(t + \Delta t) &= \mathcal{N}_P [Q(t), \text{diag}(\rho(t)) | \phi_P, \theta_P], \\ \rho_{\text{pred}}(t + \Delta t) &= \mathcal{N}_\rho [Q(t), \rho(t) | \phi_\rho, \theta_\rho]. \end{aligned} \quad (12)$$

Where $Q_{\text{pred}}(t + \Delta t)$ represents the approximation by \mathcal{N}_Q of Q at time $t + \Delta t$. We note that only the diagonal array of ρ is fed into the \mathcal{N}_P network. Starting from initial conditions $Q(0)$, $P(0)$, and $\rho(0)$, the time evolution of the Holstein model is obtained by recurrently invoking the three PARC neural networks. Our implementation of the three PARC neural nets are similar to that discussed in Ref. [17]. As discussed above, each PARC model is composed of a differentiator CNN connected to an integrator CNN. Similar structure is used for both CNNs: it is composed of two ResNet blocks [46] followed by a 7×7 convolution layer for feature extraction, two 1×1 convolution layers which further develop relationships only within each channel, and a final 3×3 convolution layer.

The training dataset was obtained from direct numerical simulations of the semiclassical Holstein model. Specifically, the standard fourth-order Runge-Kutta

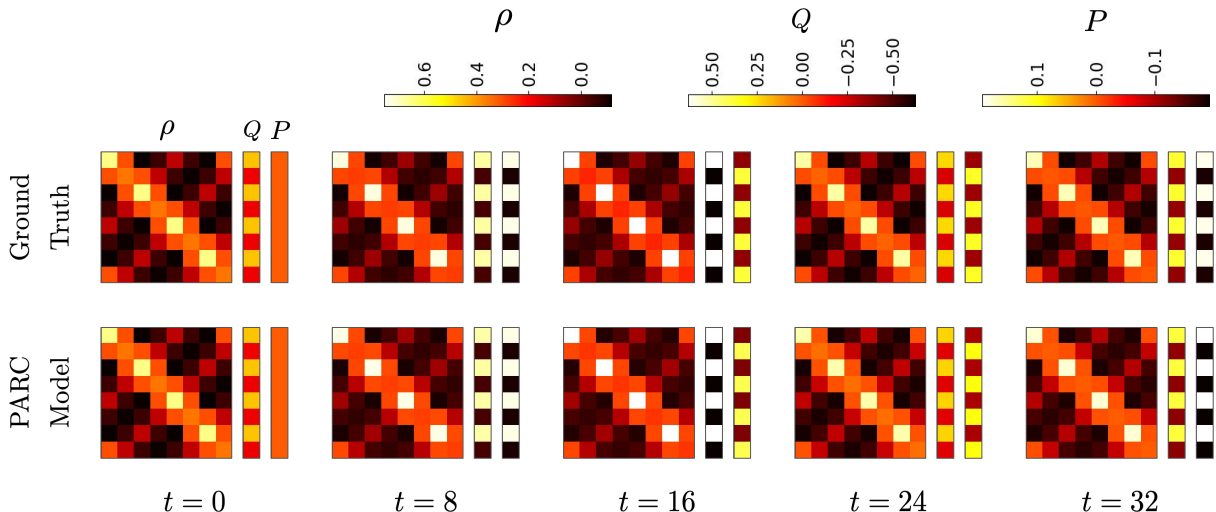


FIG. 2. Snapshots of phonon displacements Q_i , momentum P_i , and electron density matrix ρ_{ij} at various times after a shallow quench from $g_i = 0.5$ to $g_f = 0.8$ of the semiclassical Holstein model on a $L = 8$ chain. The ground truth on the top row is obtained from the 4th-order Runge-Kutta integration of the governing dynamics Eqs. (3) and (6). The bottom row shows predictions from the trained PARC model.

method was used to integrate the coupled Newton equation (3) for classical phonons and the von Neumann equation (6) for the electron density matrix. For each simulation, a total of 2500 snapshots were generated for integration from $t = 0$ to $t = 200$ with a step size of $\Delta t = 0.08$.

We consider two scenarios of interaction quench for generating the datasets. In the first case, which is referred to as the shallow quench scenario, the system is prepared in the CDW ground state stabilized by a finite electron-phonon coupling $g_i > 0$. The coupling is suddenly increased to a larger value $g_f > g_i$ at the time instance $t = 0$. This sudden increase of the interaction strength induces a transient coherent oscillation of the CDW order parameter, a nonequilibrium dynamical phenomenon that has been observed in the interaction quench of several symmetry-breaking systems including CDW, spin-density wave, and superconductivity. Moreover, we also find that the time evolution of the system after a shallow quench is nearly deterministic. As a result, the same “trajectory” is used as the training set, validation set, and test set. The aim of this data is to establish an upper-bound for the model’s ability to memorize a trajectory for use in comparison to the model’s generalization capabilities.

In the second scenario, the coupling is initially turned off $g_i = 0$, which means the corresponding ground state is free electron gas on a chain decoupled from a set of independent simple harmonic oscillators in equilibrium $Q_i = P_i = 0$. Naturally, there is no CDW order in this initial state. The electron-phonon coupling is then suddenly switch on to $g_f > 0$ at time $t = 0$. The quench dynamics in this scenario is dominated by the emergence of CDW orders induced by the nonzero g_f . The onset of

the CDW order is a stochastic process. First local CDW order is initiated through nucleation process at random seeds. This is then followed by the growth and merger of CDW domains. This scenario is akin to the phase-ordering process when a system is suddenly quenched from a high-temperature random state into a symmetry-breaking phase. As a result, the deep-quench process is very sensitive to random fluctuations in the initial states. For a controlled approach to generate dataset, Q_i are sampled from a normal distribution of zero mean and a standard deviation of 10^{-4} . Contrary to the shallow quench scenario discussed above, a wide variety of dataset with different system trajectories can be generated from the deep quench simulations.

Given the dataset in the form of exact system trajectories $\hat{\mathbf{u}}(t) = [\hat{Q}(t), \hat{P}(t), \hat{\rho}(t)]$, the loss function defined in Eq. (11) is used to obtain the optimal parameters ϕ^* and θ^* through gradient-descent training. The AdamW optimizer [47], which is a variant of the popular Adaptive Moment Estimation (Adam) algorithm [48], is used for gradient descent minimization of the loss function. In AdamW, the weight decay, a technique to preventing overfitting by penalizing large weights in neural nets, is handled more efficiently. This can help to improve model generalization as large weight values can often indicate a model is “relying” on specific, memorized features within training data instead of properly generalizing. Along with AdamW we also use a learning-rate warm-up, which gradually increases the learning rate from 0 to its set value. Because AdamW relies on estimates of the first and second moments of gradient, utilizing a warm-up decreases the learning-rate of AdamW until it has learned appropriate initial estimates for these values.

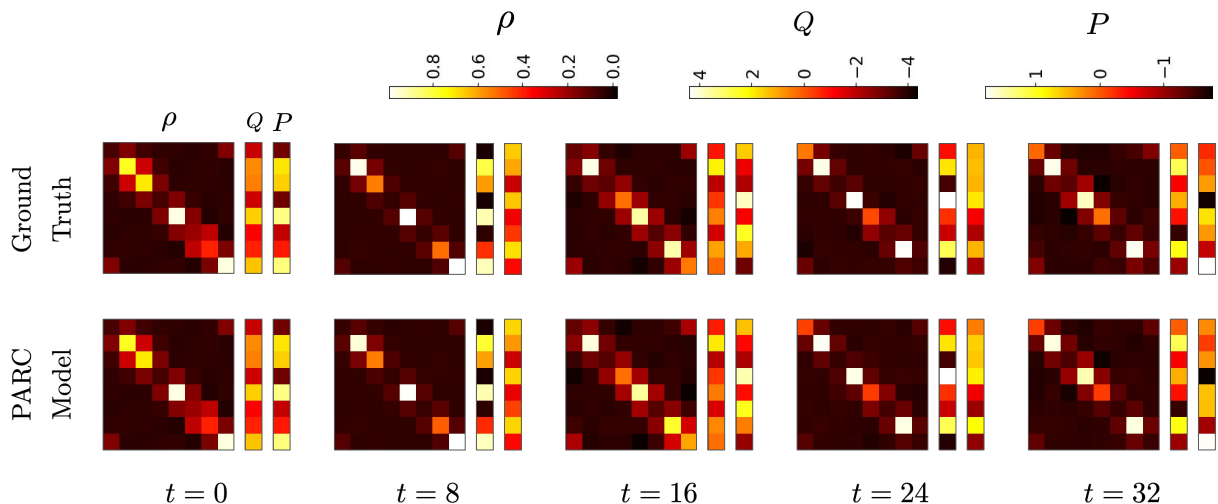


FIG. 3. Snapshots of phonon displacements Q_i , momentum P_i , and electron density matrix ρ_{ij} at various times after a deep quench from $g_i = 0$ to $g_f = 2.0$ of the semiclassical Holstein model on a $L = 8$ chain. The ground truth on the top row is obtained from the 4th-order Runge-Kutta integration of the governing dynamics Eqs. (3) and (6). The bottom row shows predictions from the trained PARC model.

In accordance with [49], we utilize channel-wise dropout instead of element-wise dropout. Traditional element-wise dropout, when placed between two layers of a neural network, helps to regularize by setting a random proportion of incoming values to zero (hence “dropout”) during training. This forces the next layer to use a different subset of the incoming information each time by reducing reliance on only specific parts of the information. However, this random dropout of all values can introduce noise to convolution layers by interfering with local relationships, thereby reducing overall effectiveness. Channel-wise dropout addresses this by dropping out entire channels in a convolution layer, thereby fully preserving important locality information in the remaining channels.

IV. RESULTS

FIG. 2 shows the comparison of PARC simulation and ground truth for the time evolution of a $L = 8$ system subject to a shallow quench from $g_i = 0.5$ to $g_f = 0.8$ at time $t = 0$. The ground truth was obtained from integration with the 4th-order Runge-Kutta (RK4) method. A time-step $\Delta t = 0.08$ was used both in the RK4 integration and the PARC prediction; the simulation from $t = 0$ to $t = 32$ thus corresponds to 400 iterations of predictions from the model. As discussed above, the system is initially in a CDW state where the on-site electron number $n_i = \rho_{ii}$ exhibits an alternating $\bar{n} + \delta n$ and $\bar{n} - \delta n$ pattern along the chain with the period of one lattice constant. This is accompanied by a $\pm Q_0$ modulation due to the finite electron-phonon coupling g_i . After the quench, the relaxation of the system towards the shifted ground state

induces a coherent oscillation. Importantly, during this coherent regime, the system remains in a perfect CDW state with a time-varying modulation amplitude. Our benchmark shows that the PARC predictions accurately captures the coherent oscillation dynamics in all three Q , P , and ρ sectors.

Next we consider the deep quench scenario, where an initial state of decoupled electrons and phonons (corresponding to $g_i = 0$) is perturbed by a switch-on of the electron-phonon coupling. The comparison of the ground truth and the PARC prediction is shown in FIG. 3. To demonstrate the generalization capability of the PARC model, an arbitrary nonequilibrium state for both phonon and electron subsystems is used as the initial state. Contrary to a persistent long-range CDW order in the shallow quench case, the dynamical evolution is characterized by the presence of strong spatial fluctuations. The spatial inhomogeneity also manifests itself in the localization of electrons, giving rise to relatively small off-diagonal matrix elements in the electron density matrix ρ . As the figure shows, the rather inhomogeneous dynamical evolution is also nicely captured by the PARC model. It is also worth noting that this benchmark was done on an initial state which was not among the training dataset. This thus demonstrates the transferability of the PARC model.

Next we present systematic studies on model prediction accuracy with respect to prediction window, prediction step size, training dataset size, and complexity of NN models. To quantify the prediction accuracy, we define the RMSE of each of ρ , Q , and P on next-step prediction

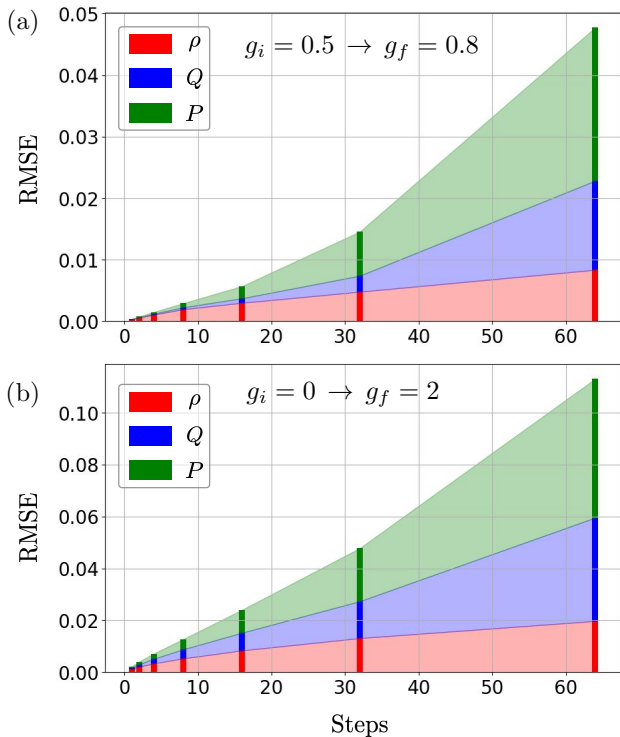


FIG. 4. RMSE versus prediction window for (a) shallow quench $g = 0.5$ to 0.8 and (b) a deep quench with $g = 0$ to 2.0 .

as follows:

$$\text{RMSE}_Q = \sqrt{\frac{[Q(t + \Delta t) - Q_{\text{pred}}(t + \Delta t)]^2}{L}}$$

$$\text{RMSE}_P = \sqrt{\frac{[P(t + \Delta t) - P_{\text{pred}}(t + \Delta t)]^2}{L}}$$

$$\text{RMSE}_\rho = \sqrt{\frac{|\rho(t + \Delta t) - \rho_{\text{pred}}(t + \Delta t)|^2}{L^2}}$$

Where L denotes the system size (the square size of ρ and length of Q and P) and $|\cdot|$ denotes *element-wise* magnitude. Then the total RMSE of next-step prediction is defined as:

$$\text{RMSE} = \text{RMSE}_\rho + \text{RMSE}_Q + \text{RMSE}_P$$

FIG. 4 shows the increase in prediction RMSE with respect to the number of steps predicted for. We can see that initial error accumulation appears to be relatively linear, but this trends exponential as the error continues to compound for greater number of steps. The magnitude of error for all step counts is around 2 times lower for model trained on shallow-quench data in FIG. 4(a) compared to the model trained on deep-quench data in FIG. 4(b).

This can be explained as the model is more capable of memorizing and overfitting to the single trajectory of

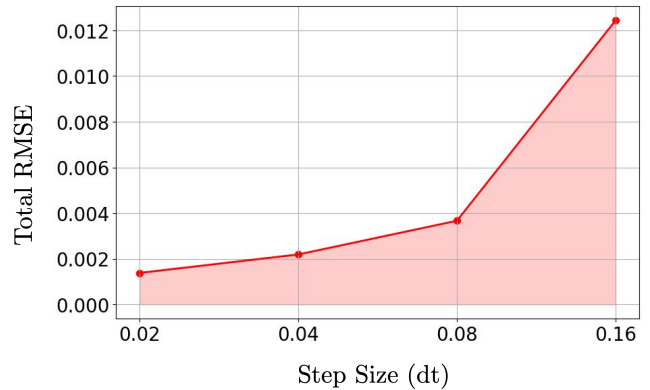


FIG. 5. Total RMSE versus the prediction step size Δt for the PARC model trained on the deep quench data.

the small quench scenario, whereas generalization is vital for the performance of the deep-quench model. As a result, the shallow-quench trained PARC model, having effectively memorized the single trajectory data, performs better on the same data than the deep-quench trained model on a test set it was not trained on. However, being less generalized itself, the single-trajectory PARC model is also less capable of handling out-of-distribution situations, which in this case takes the form of its predictions as error accumulates with step size, resulting in increasingly unfamiliar inputs. As a result, we see that while the errors of the single-trajectory model may be lower for all step counts tested, the scaling of its error with respect to step count is more exponential than that of the deep-quench trained case, which can better handle error accumulation due to increased generalization on a variety of trajectories.

We next test the scaling of the RMSE of the PARC model trained on the deep-quench data with step sizes of $\Delta t = 0.02, 0.04, 0.08, 0.16$. FIG. 5 displays the average RMSE of a model trained on a data set with a certain step size on a corresponding test set. As expected, the error increases with step size. We can see that the scaling is somewhat greater than linear, which is expected as the degree of uncertainty compounds with larger step sizes.

We also experiment with training the model on datasets containing 32, 64, 128, 256, 512, 1024, and 2048 trajectories. All models were trained with the same amount of compute to enable an even comparison. As we can see in FIG. 6, all datasets except that with 32 trajectories perform roughly evenly, indicating a sharp asymptote in the benefit of increased data diversity to generalization between datasets containing 32 trajectories to those containing 64. This shows that there is minimal practical gain to using datasets containing more than 64 trajectories, although there does not seem to be any harm in increased diversity either. The lack of harm from increased dataset size seems to imply that the model generalizes well, as it does not rely on memorization of the individual trajectories.

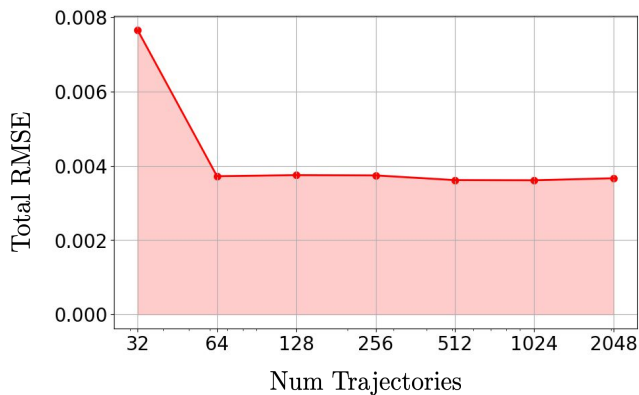


FIG. 6. Total RMSE vs size of training dataset measured by the number of deep-quench trajectories used in the training.

Finally, we examine the dependence of the prediction errors on the complexity of the PARC model. To this end, we scale the parameter count of the model by proportionally scaling the number of channels within each convolution layer of PARC. By default, PARC has 128 channels in its convolution with the greatest number of channels. We test scaling which results in 32, 64, 128, and 256 channels at the convolution with greatest channel count. FIG. 7 shows the RMSE of such models on a test set against their total parameter count. As expected, the RMSE of the model decreases as the capacity of the model increases. This indicates that increasing the size of the model is an avenue for increased performance. However, we can also see from the figure, which has a logarithmic horizontal axis, that the benefit derived from increased size exhibits sublinear scaling and, as the total RMSE of prediction can only ever approach 0, exhibits diminishing returns as parameter count increases. Beyond a certain point it is likely ineffective or impractical to continue scaling the model due to the trade-off between performance and training/inference.

V. SUMMARY AND OUTLOOK

We have demonstrated the efficacy of a PARC-based recurrent CNN model to capture the time evolution of a one-dimensional semiclassical Holstein model under a quantum interaction quench. Within the Ehrenfest dynamics formalism, the non-adiabatic dynamics of the Holstein model is governed by the classical equation of motion for phonons, described by a set of simple harmonic oscillators and the von Neumann equation for the reduced density matrix of electrons. Leveraging the capability of CNNs to learn hierarchical local spatial correlations, our model is capable of generalizing to the integration of solutions to unseen initial conditions. The task of integration approximation is further augmented by the explicit differentiator-integrator structure of the

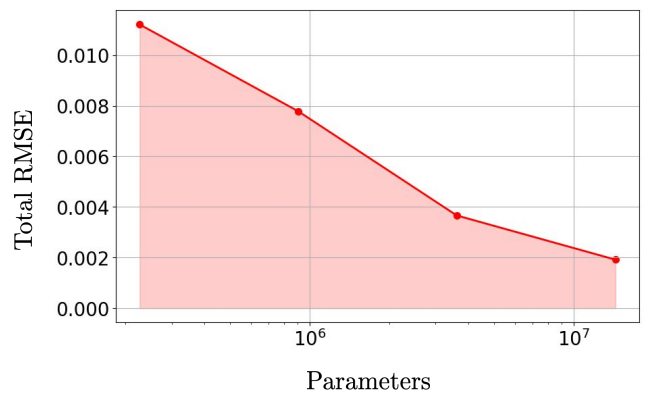


FIG. 7. Total RMSE vs parameters of the CNN in the PARC model.

PARC model, which integrates a physics-aware prior into the architecture. By utilizing a recurrent, next-step prediction target, our model is capable of predicting many steps of integration given any starting point.

Our benchmark studies on two quench scenarios have also demonstrated the accuracy of predicted trajectories to ground-truth. Because our model utilizes three separate CNNs for the density matrix, displacement vector, and momentum vector in the Holstein system, this indicates that each CNN has separately learned to appropriately capture the rules of integration for its corresponding equation in the system of PDEs from only the data. Additionally, we have explored the error accumulation with continued recurrent predictions and scaling properties of the step size of the data, size of the training set, and size of the model on the error of the prediction. Through these analyses we have been able to deduce effective model configurations and areas of diminishing returns.

A current area for improvement could be the long-term prediction accuracy of the model, and this could serve as a valuable subject for extension. For example, techniques used to increase the effective context window of RNNs could be applied, or even hybrid approaches such as integrating weak PINN constraints to the system.

The semiclassical Holstein model studied in this work serves as a proof-of-concept for demonstrating the capability of PARC in learning non-adiabatic dynamics hybrid quantum-classical systems. The PARC framework can in principle be applied to other more complex quantum-classical systems, in particular the non-adiabatic quantum molecular dynamics. As discussed above, even for non-interacting electron systems, a minimum description in terms of single-particle reduced density matrix is required in order to account for the quantum Fermi-Dirac statistics. This means that the dynamics of a D -dimensional hybrid quantum-classical system can be modeled as $2D$ -dimensional classical differential equations. For more complex systems with genuine electron-electron interactions, more sophisticated meth-

ods, depending on approximations used, are required to describe the time-evolution of the quantum subsystem. An intriguing possibility is that the PARC model can be trained to learn the effective dynamics of the reduced single-electron density matrix, even though it is not described by an explicit von Neumann equation.

ACKNOWLEDGMENTS

The work was supported by the US Department of Energy Basic Energy Sciences under Contract No. DE-

SC0020330. L. Yang acknowledges the support of Jefferson Fellowship. GWC thanks Phong Nguyen and Stephen Baek for useful discussions on PARC neural networks, as well as Changnan Peng, Jin-Peng Liu, and Di Luo for insightful discussions on quantum dynamics and collaboration on a related project regarding adiabatic dynamics. The authors also acknowledge the support of Research Computing at the University of Virginia.

-
- [1] S. Hochreiter and J. Schmidhuber, Long short-term memory, *Neural Computation* **9**, 1735 (1997).
- [2] A. Graves, Supervised sequence labelling, in *Supervised Sequence Labelling with Recurrent Neural Networks* (Springer, New York, 2012) pp. 5–13.
- [3] Z. C. Lipton, J. Berkowitz, and C. Elkan, [A critical review of recurrent neural networks for sequence learning](#) (2015), [arXiv:1506.00019 \[cs.LG\]](#).
- [4] A. Sherstinsky, Fundamentals of recurrent neural network (rnn) and long short-term memory (lstm) network, *Physica D: Nonlinear Phenomena* **404**, 132306 (2020).
- [5] Y. Hu, T. Zhao, S. Xú, L. Lin, and Z. Xu, Neural-pde: a rnn based neural network for solving time dependent pdes, *Commun. Inf. Syst.* **22**, 223 (2020).
- [6] M. Karlbauer, T. Praditia, S. Otte, S. Oladyshkin, W. Nowak, and M. V. Butz, Composing partial differential equations with physics-aware neural networks, in *International Conference on Machine Learning* (PMLR, 2022) pp. 10773–10801.
- [7] A. M. Hafiz, I. Faiq, and M. Hassaballah, Solving partial differential equations using large-data models: a literature review, *Artificial Intelligence Review* **57**, 152 (2024).
- [8] B. Wu, O. Hennigh, J. Kautz, S. Choudhry, and W. Byeon, Physics informed rnn-dct networks for time-dependent partial differential equations, in *Computational Science – ICCS 2022*, edited by D. Groen, C. de Mulatier, M. Paszynski, V. V. Krzhizhanovskaya, J. J. Dongarra, and P. M. A. Sloot (Springer International Publishing, Cham, 2022) pp. 372–379.
- [9] Y. Sun, L. Zhang, and H. Schaeffer, NeuPDE: Neural network based ordinary and partial differential equations for modeling time-dependent data, in *Proceedings of The First Mathematical and Scientific Machine Learning Conference*, Proceedings of Machine Learning Research, Vol. 107, edited by J. Lu and R. Ward (PMLR, 2020) pp. 352–372.
- [10] Q. Zhong, Y. Sun, and Z. Qiu, Deep recurrent neural network with sharing weights for solving high-dimensional pdes, in *2021 IEEE International Conference on Data Science and Computer Application (ICDSCA)* (2021) pp. 6–9.
- [11] Y. Liang, R. Niu, J. Yue, and M. Lei, A physics-informed recurrent neural network for solving time-dependent partial differential equations, *International Journal of Computational Methods* **21**, 2341003 (2024).
- [12] Z. Long, Y. Lu, X. Ma, and B. Dong, PDE-net: Learning PDEs from data, in *Proceedings of the 35th International Conference on Machine Learning*, Proceedings of Machine Learning Research, Vol. 80, edited by J. Dy and A. Krause (PMLR, 2018) pp. 3208–3216.
- [13] Z. Long, Y. Lu, and B. Dong, Pde-net 2.0: Learning pdes from data with a numeric-symbolic hybrid deep network, *Journal of Computational Physics* **399**, 108925 (2019).
- [14] Z. Zuo, B. Shuai, G. Wang, X. Liu, X. Wang, B. Wang, and Y. Chen, Convolutional recurrent neural networks: Learning spatial dependencies for image representation, in *2015 IEEE Conference on Computer Vision and Pattern Recognition Workshops (CVPRW)* (2015) pp. 18–26.
- [15] P. Saha, S. Dash, and S. Mukhopadhyay, Physics-incorporated convolutional recurrent neural networks for source identification and forecasting of dynamical systems, *Neural Networks* **144**, 359 (2021).
- [16] P. Ren, C. Rao, Y. Liu, J.-X. Wang, and H. Sun, Phycrnet: Physics-informed convolutional-recurrent network for solving spatiotemporal pdes, *Computer Methods in Applied Mechanics and Engineering* **389**, 114399 (2022).
- [17] P. C. Nguyen, Y.-T. Nguyen, J. B. Choi, P. K. Seshadri, H. S. Udaykumar, and S. S. Baek, PARC: Physics-aware recurrent convolutional neural networks to assimilate meso scale reactive mechanics of energetic materials, *Science Advances* **9**, eadd6868 (2023).
- [18] P. C. H. Nguyen, X. Cheng, S. Azarfar, P. Seshadri, Y. T. Nguyen, M. Kim, S. Choi, H. S. Udaykumar, and S. Baek, [PARCv2: Physics-aware recurrent convolutional neural networks for spatiotemporal dynamics modeling](#) (2024), [arXiv:2402.12503 \[cs.LG\]](#).
- [19] W. H. Press, S. A. Teukolsky, W. T. Vetterling, and B. P. Flannery, *Numerical Recipes in C*, 2nd ed. (Cambridge University Press, Cambridge, USA, 1992).
- [20] K. W. Morton and D. F. Mayers, *Numerical Solution of Partial Differential Equations: An Introduction*, 2nd ed. (Cambridge University Press, 2005).
- [21] U. M. Ascher, S. J. Ruuth, and R. J. Spiteri, Implicit-explicit runge-kutta methods for time-dependent partial differential equations, *Applied Numerical Mathematics* **25**, 151 (1997), special Issue on Time Integration.
- [22] I. Goodfellow, Y. Bengio, and A. Courville, Convolutional networks, in *Deep Learning* (MIT Press, 2016) Chap. 9, pp. 326–366.
- [23] J. Behler and M. Parrinello, Generalized neural-network representation of high-dimensional potential-energy surfaces, *Phys. Rev. Lett.* **98**, 146401 (2007).

- [24] A. P. Bartók, M. C. Payne, R. Kondor, and G. Csányi, Gaussian approximation potentials: The accuracy of quantum mechanics, without the electrons, *Phys. Rev. Lett.* **104**, 136403 (2010).
- [25] Z. Li, J. R. Kermode, and A. De Vita, Molecular dynamics with on-the-fly machine learning of quantum-mechanical forces, *Phys. Rev. Lett.* **114**, 096405 (2015).
- [26] A. V. Shapeev, Moment tensor potentials: A class of systematically improvable interatomic potentials, *Multiscale Modeling & Simulation* **14**, 1153 (2016).
- [27] V. Botu, R. Batra, J. Chapman, and R. Ramprasad, Machine learning force fields: Construction, validation, and outlook, *The Journal of Physical Chemistry C* **121**, 511 (2017).
- [28] S. Chmiela, A. Tkatchenko, H. E. Sauceda, I. Poltavsky, K. T. Schütt, and K.-R. Müller, Machine learning of accurate energy-conserving molecular force fields, *Science Advances* **3**, e1603015 (2017).
- [29] S. Chmiela, H. E. Sauceda, K.-R. Müller, and A. Tkatchenko, Towards exact molecular dynamics simulations with machine-learned force fields, *Nature Communications* **9**, 3887 (2018).
- [30] M. Weiler, M. Geiger, M. Welling, W. Boomsma, and T. S. Cohen, 3d steerable cnns: Learning rotationally equivariant features in volumetric data, *Advances in Neural Information Processing Systems* **31** (2018).
- [31] S. Batzner, A. Musaelian, L. Sun, M. Geiger, J. P. Mailoa, M. Kornbluth, N. Molinari, T. E. Smidt, and B. Kozinsky, E(3)-equivariant graph neural networks for data-efficient and accurate interatomic potentials, *Nature Communications* **13**, 2453 (2022).
- [32] X. Gong, H. Li, N. Zou, R. Xu, W. Duan, and Y. Xu, General framework for e(3)-equivariant neural network representation of density functional theory hamiltonian, *Nature Communications* **14**, 2848 (2023).
- [33] P. Ma, P. Y. Chen, B. Deng, J. B. Tenenbaum, T. Du, C. Gan, and W. Matusik, Learning neural constitutive laws from motion observations for generalizable pde dynamics, in *Proceedings of the 40th International Conference on Machine Learning, ICML'23 (JMLR.org, 2023)*.
- [34] D. Marx and J. Hutter, *Ab initio molecular dynamics: basic theory and advanced methods* (Cambridge University Press, 2009).
- [35] X. Cheng, S. Zhang, P. C. H. Nguyen, S. Azarfar, G.-W. Chern, and S. S. Baek, Convolutional neural networks for large-scale dynamical modeling of itinerant magnets, *Phys. Rev. Res.* **5**, 033188 (2023).
- [36] G. E. Karniadakis, I. G. Kevrekidis, L. Lu, P. Perdikaris, S. Wang, and L. Yang, Physics-informed machine learning, *Nature Reviews Physics* **3**, 422 (2021).
- [37] M. Raissi, P. Perdikaris, and G. Karniadakis, Physics-informed neural networks: A deep learning framework for solving forward and inverse problems involving nonlinear partial differential equations, *Journal of Computational Physics* **378**, 686 (2019).
- [38] T. Holstein, Studies of polaron motion: Part i. the molecular-crystal model, *Annals of Physics* **8**, 325 (1959).
- [39] R. M. Noack, D. J. Scalapino, and R. T. Scalettar, Charge-density-wave and pairing susceptibilities in a two-dimensional electron-phonon model, *Phys. Rev. Lett.* **66**, 778 (1991).
- [40] Y.-X. Zhang, W.-T. Chiu, N. C. Costa, G. G. Batrouni, and R. T. Scalettar, Charge order in the holstein model on a honeycomb lattice, *Phys. Rev. Lett.* **122**, 077602 (2019).
- [41] C. Chen, X. Y. Xu, Z. Y. Meng, and M. Hohenadler, Charge-density-wave transitions of dirac fermions coupled to phonons, *Phys. Rev. Lett.* **122**, 077601 (2019).
- [42] I. Esterlis, S. A. Kivelson, and D. J. Scalapino, Pseudogap crossover in the electron-phonon system, *Phys. Rev. B* **99**, 174516 (2019).
- [43] X. Li, J. C. Tully, H. B. Schlegel, and M. J. Frisch, Ab initio ehrenfest dynamics, *The Journal of Chemical Physics* **123**, 084106 (2005).
- [44] M. D. Petrovic, M. Weber, and J. K. Freericks, Theoretical description of time-resolved photoemission in charge-density-wave materials out to long times (2022), [arXiv:2203.11880 \[cond-mat.str-el\]](https://arxiv.org/abs/2203.11880).
- [45] L. Lu, P. Jin, G. Pang, Z. Zhang, and G. E. Karniadakis, Learning nonlinear operators via deeponet based on the universal approximation theorem of operators, *Nature Machine Intelligence* **3**, 218 (2021).
- [46] K. He, X. Zhang, S. Ren, and J. Sun, Deep residual learning for image recognition, in *2016 IEEE Conference on Computer Vision and Pattern Recognition (CVPR)* (2016) pp. 770–778.
- [47] I. Loshchilov and F. Hutter, Decoupled weight decay regularization, in *International Conference on Learning Representations* (2017).
- [48] D. P. Kingma and J. Ba, Adam: A method for stochastic optimization (2017), [arXiv:1412.6980 \[cs.LG\]](https://arxiv.org/abs/1412.6980).
- [49] J. Tompson, R. Goroshin, A. Jain, Y. LeCun, and C. Bregler, Efficient object localization using convolutional networks, *2015 IEEE Conference on Computer Vision and Pattern Recognition (CVPR)*, 648 (2014).